GEOPHYSICS, VOL. 70, NO. 3 (MAY-JUNE 2005); P. V81–V86, 4 FIGS.
10.1190/1.1926578

Short Note

Approximate separation of pure-mode and converted waves in 3-C reflection seismics by τ-p transform

Abdullah Al-anboori[1], Mirko van der Baan[1], and J. Michael Kendall[1]

INTRODUCTION

The use of multicomponent receivers allows one to record the complete elastic wavefield. This is desirable since knowledge of both P- and S-wave characteristics yields better insights into subsurface lithologic and structural rock properties than P-wave knowledge alone. It is often assumed in multicomponent processing that the vertical z-component contains principally pure-mode P-wave arrivals and that the inline horizontal x-component consists mainly of P-SV converted-wave energy. This assumption actually becomes worse with increasing offset. Contaminating energy on either component should ideally be removed to prevent degeneration of stack quality. Often, the x-component is more contaminated than the z-component because P-wave incidence angles (from vertical) are larger than those of P-S waves. This renders processing of the x-component more challenging. Removal of contaminating energy on either component may lead to sharper images. One way of removing such undesired energy is by means of wavefield separation. We propose a simple, approximate wavefield-separation scheme in the τ-p domain to better isolate pure-mode and converted-wave signals.

Broadly speaking, techniques for wavefield separation fall into two categories: wave-theoretical methods (Dankbaar, 1985; Greenhalgh et al., 1990; Wapenaar et al., 1990; Amundsen and Reitan, 1995; Wang and Singh, 2002) and parametric methods (Esmersoy, 1990; Cho and Spencer, 1992). Exact wave-theoretical methods are directly based on the physics of wave propagation but require the specification of both P- and S-wave near-surface velocities for land data and additional density parameters for ocean-bottom cable (OBC) data. Parametric methods, on the other hand, do not require a priori information about the near-surface layer. However, they assume that impinging waves are locally planar (that is, characterized by a constant slowness) and that receiver spacing is sufficiently dense such that robust estimates of local slownesses and polarization angles can be made. They require, therefore, specification of the width and length of a local data-analysis window and sometimes even an estimate of the number of waves to be expected (Richwalski et al., 2000). They cannot deal with more complex wave-propagation phenomena, e.g., the free-surface effect.

We present a simplified version of the separation scheme of Greenhalgh et al. (1990). Our approximate wave-theoretical separation scheme is based on a data rotation in the τ-p domain to remove to a large extent either contaminating P-P pure-mode waves on the x-component or P-SV converted-wave energy on the z-component. Our scheme has the advantage over exact wavefield-separation schemes in that only a single parameter needs to be specified; namely, the near-surface P-wave velocity v_p for P-S wave enhancement or, conversely, the near-surface S-wave velocity v_s for P-P energy enhancement.

In this paper, we describe the technique and perform sensitivity tests on synthetic data to demonstrate its robustness. We end with a real data example.

THEORY

The separation scheme is based on a simple rotation of data recorded in Cartesian coordinates (x, z) to ray coordinates (l, n) using the incidence angle of the wave. The data have been previously rotated into the in-line x- and crossline y-coordinates. By convention, the l-component is the longitudinal direction along the ray, and the n-component is normal to the ray while lying within the sagittal plane. The displacements on the x- and z-components are denoted by $u_x(t, x)$ and $u_z(t, x)$, respectively. We assume that P- and P-S waves are entirely polarized in the x-z plane and that their polarization is either parallel (P-waves) or perpendicular (S-waves) to their ray-propagation direction (Figure 1).

Manuscript received by the Editor October 29, 2003; revised manuscript received June 2, 2004; published online May 20, 2005.
[1]University of Leeds, School of Earth Sciences, Leeds LS2 9JT, United Kingdom. E-mail: anboori@earth.leeds.ac.uk; mvdbaan@earth.leeds.ac.uk; kendall@earth.leeds.ac.uk.

Such a rotation is not easily implemented in the x-t domain because each trace contains multiple arrivals with time-varying incidence angles. However, a similar rotation can be applied on τ-p gathers, $S_x(\tau, p)$ and $S_z(\tau, p)$, where data are sorted into horizontal slowness p and intercept time τ (Stoffa et al., 1981). The incidence angle θ can be computed from the horizontal slowness p using Snell's law if we assume that a thin, laterally homogeneous, near-surface layer exists. That is, $\theta = \sin^{-1}(pv_1)$, where v_1 is the near-surface velocity of the considered wave mode. The gathers $S_x(\tau, p)$ and $S_z(\tau, p)$ correspond to the τ-p transformed shot gathers $u_x(t, x)$ and $u_z(t, x)$, respectively. The gathers $S_x(\tau, p)$ and $S_z(\tau, p)$ are then rotated by the incidence angle θ to ray-parallel $S_l(\tau, p)$ and ray-perpendicular $S_n(\tau, p)$ gathers using a rotation matrix:

$$\begin{pmatrix} S_n(\tau, p) \\ S_l(\tau, p) \end{pmatrix} = \begin{pmatrix} \cos\theta & -\sin\theta \\ \sin\theta & \cos\theta \end{pmatrix} \begin{pmatrix} S_x(\tau, p) \\ S_z(\tau, p) \end{pmatrix}. \quad (1)$$

The advantage of this approach is that the appropriate rotation angle depends only on the wave mode but does not vary over time for a given constant-slowness trace. We now require only knowledge of the mode of the detected arrival (i.e., P-P or P-S waves) so that an exact separation scheme can be devised that depends on both the near-surface P-wave, v_p, and S-wave, v_s, velocities and, additionally, density for OBC data (Wang and Singh, 2002).

On the other hand, we could assume that all recorded energy consists of pure-mode P-P arrivals only and use the near-surface v_p to determine the P-wave rotation angle θ_p using Snell's law. After rotation, the l-component will actually contain all P-wave energy plus some converted waves. This rotated component is called the pass plane in the terminology of Greenhalgh et al. (1990). The resulting n-component, called the extinction plane, is free of P-P wave energy (Figure 1b). An inverse τ-p transform applied on the n-component now results in a converted-wave gather free of any interfering P-P wave arrivals. The resulting displacements after inverse τ-p transform on the l- and n-component are denoted $u_l(t, x)$ and $u_n(t, x)$, respectively.

Similarly, the same procedure using the near-surface S-wave velocity v_s yields improved P-P gathers (Figure 1c). Only a single near-surface velocity is required for S/N enhancement, namely, v_p to fully eliminate P-waves and v_s to fully reject S-waves. The scheme assumes an elastic, isotropic, and homogeneous surface layer and negligible free-surface effects. Free-surface effects of incident P-S waves are much less pronounced than those of P-waves because of steeper incidence angles. Fortunately, free-surface effects are most dominant for large offset/depth ratios which, in practice, are nearly always muted out. The separation scheme is therefore applicable to a laterally inhomogeneous anisotropic earth with an overlying homogeneous isotropic surface layer. However, wavefield separation is performed on the final wave mode as recorded at the receiver level, i.e., locally converted waves are not extracted unless they arrive as S-waves at the surface.

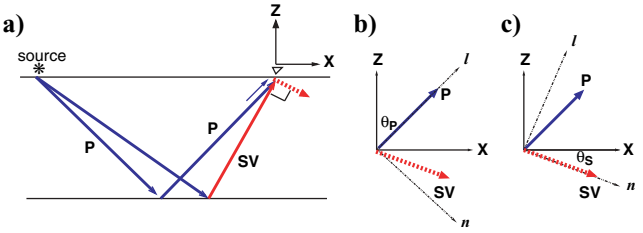

Figure 1. (a) P-P and P-S wave ray paths and their polarization vectors for a simple one-layer model. The data is rotated from general Cartesian coordinates (x, z) to ray coordinates (l, n) using (b) the near-surface P-wave velocity v_p or (c) the S-wave velocity v_s. The l- and n-components are, respectively, along and perpendicular to the ray direction while remaining within the sagittal plane. The angles θ_p and θ_s indicate the P-P- and P-S-wave incidence angles, respectively.

Our approach is similar to the one proposed by Greenhalgh et al. (1990) except that they use the same rotation technique as a preprocessing step to determine the pass plane, followed by a linear polarization filter to remove any remaining unwanted energy. The latter step is related to parametric wavefield-separation techniques and suffers from the same inconveniences. We, on the other hand, content ourselves with the extinction plane to approximately separate P-P and P-S waves at the surface.

The separation technique does not recover the entire incident-wave amplitude except at vertical incidence (i.e., zero slowness) because of the nonorthogonality of the P- and P-S wave particle motion for identical horizontal slownesses. The performance of the separation scheme actually degrades with increasing slowness p and, therefore, offset. The amount of recovered energy in the extinction plane can be computed analytically (Greenhalgh et al., 1990). The ratio of the recovered P-wave amplitude $u_{P,l}$ as projected on the l-axis to the total incident P-wave amplitude $u_{P,tot}$ and the ratio of the recovered S-wave amplitude $u_{S,n}$ on the n-axis to the total incident P-S wave amplitude $u_{S,tot}$ are both given by $\cos(\theta_p - \theta_s)$ (Figures 1b and 1c). That is,

$$\frac{u_{P,l}}{u_{P,tot}} = \frac{u_{S,n}}{u_{S,tot}} = \cos(\theta_p - \theta_s) = v_p v_s \left[q_p q_s + p^2\right], \quad (2)$$

where q_p and q_s denote the vertical P- and S-wave slownesses and are given by $q_p = (v_p^{-2} - p^2)^{1/2}$ and $q_s = (v_s^{-2} - p^2)^{1/2}$.

It can be shown from equation 2 that the separation quality decreases with increasing slowness but depends also on the actual v_p/v_s ratio. The quality increases with decreasing v_p/v_s ratio. For instance, more than 90% of the amplitudes is recovered for $p < 0.5$ s/km, $v_p/v_s = \sqrt{3}$, and $v_p = 1.6$ km/s. This corresponds to P-wave incidence angles less than 53° and S-wave angles up to 28° and, therefore, offset/depth ratios of 2.7 and 1.8, respectively, for a one-layer medium.

APPLICATION TO SYNTHETIC DATA

An isotropic 1D earth model composed of six layers is employed to study the performance of our separation method. The velocities are monotonically increasing with depth with a roughly constant v_p/v_s ratio of $\sqrt{3}$. The near-surface v_p and v_s are 1.6 km/s and 0.9 km/s, respectively. All common-shot gathers (CSGs) are computed by ray tracing (Guest and Kendall, 1993) using a P-wave source with maximum offsets of 4 km and a receiver spacing of 25 m. A Ricker wavelet with a dominant frequency of 20 Hz is used. Only primary P-P and P-S wave reflections are computed.

Figure 2 shows, step by step, application of the scheme to the CSG u_x and u_z to remove P-wave contamination on the

x-component using the near-surface P-wave velocity v_p. First, u_z and u_x are transformed to the τ-p domain, producing the gathers S_z and S_x. Then, these are rotated to longitudinal and normal components S_l and S_n using Snell's law and expression 1. An inverse τ-p transform produces the new shot gathers $u_l(x, t)$ and $u_n(x, t)$. As predicted, the reconstructed shot gather u_n is free of P-wave contamination (compare Figures 2b and 2h). Even overlapping P-S and P arrivals are well separated. Using v_s instead of v_p produces a new P-P wave shot gather $u_l(x, t)$ that is free of P-S wave contamination.

SENSITIVITY AND ACCURACY TESTS

Sensitivity tests are carried out to determine to what accuracy the near-surface velocity needs to be specified and to investigate the effects of lateral velocity gradients and anisotropy in the first layer.

Relative error in v_p and v_s

It is not always easy to accurately determine the near-surface velocities v_p and v_s. An incorrect estimate of v_p causes P-wave spillover on the n-component as a result of incorrect estimation of the P-wave incidence angle θ_p. The P-wave spillover can be analytically calculated as a function of percentage error in v_p. The amount of P-wave spillover on the n'-component $u'_{P,n}$ as a fraction of $u_{P,tot}$ created by an erroneous velocity v'_p is given by

$$\frac{u'_{P,n}}{u_{P,tot}} = sin(\theta'_p - \theta_p) = v_p v'_p p(q_p - q'_p), \qquad (3)$$

where θ'_p is the erroneous incidence angle of the P-wave and $q'_p = (v'^{-2}_p - p^2)^{1/2}$. Misspecification of v_p also leads to an increase or decrease in S-wave energy recovered on the n-component, depending on the sense of the error. The recovered amount of S-wave energy $u'_{S,n}$ is given by expression 2 with θ_p replaced with θ'_p. Therefore, the amplitude ratio $u'_{P,n}/u'_{S,n}$ indicates simultaneously how P-wave energy spills over and how S-wave energy is changed on what otherwise would have been a gather containing S-wave energy only. It is given by

$$\frac{u'_{P,n}}{u'_{S,n}} = \frac{u_{P,tot}}{u_{S,tot}} \frac{v_p}{v_s} \frac{p(q_p - q'_p)}{(q'_p q_s + p^2)}. \qquad (4)$$

Analysis of equation 4 shows that P-wave spillover increases with increasing v_p percentage error and slowness. However, for a given absolute v_p percentage error, overestimated v_p leaks more P-wave energy than underestimated v_p. It also depends less significantly on the v_p/v_s ratio as P-wave spillover increases with increasing

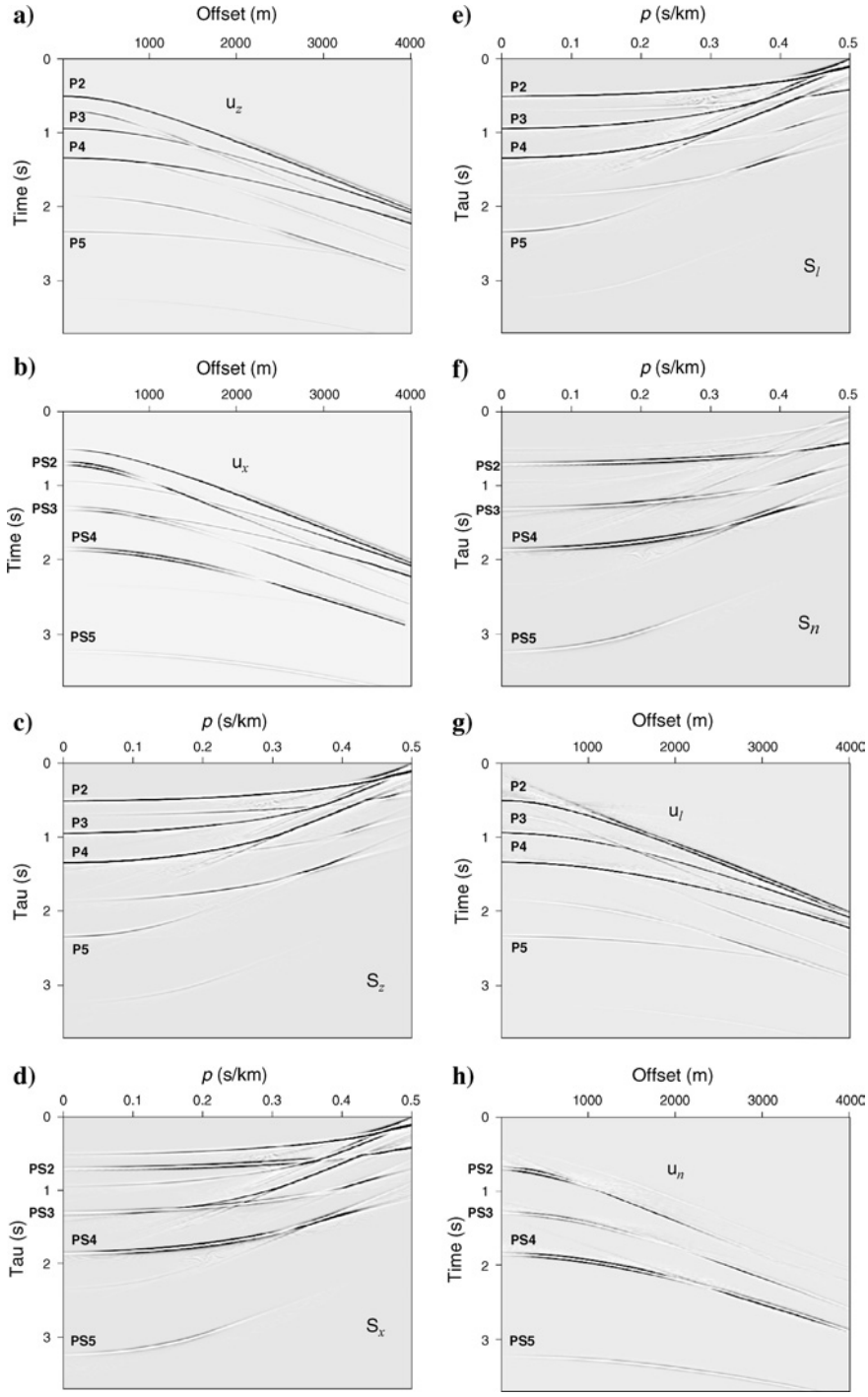

Figure 2. Illustration of the rotation procedure using the near-surface P-wave velocity to remove P-waves. Shot gathers u_z (a) and u_x (b) are transformed to the τ-p gathers S_z (c) and S_x (d), and rotated to longitudinal and normal components S_l (e) and S_n (f). An inverse τ-p transform then produces the new shot gathers u_l (g) and u_n (h). Nearly all P-wave energy has been removed from the extinction plane u_n [compare (b) and (h)]. Pn and PSn denote primary reflections/conversions of the nth interface, respectively. Reflections and conversions of the bottom of the weathering layer are not shown (P1 and PS1).

v_p/v_s ratio. For instance, errors up to −25% and +20% in v_p (for $p = 0.4$ s/km, $v_p/v_s = \sqrt{3}$, $v_p = 1.6$ km/s, and $u_{P,tot} = u_{S,tot}$) produce 20% P-wave spillover. The effect of v_p error on the separation quality is illustrated in Figure 3 using a +20% error in v_p. P-waves (particularly P_2) spillover onto the P-S section increases with increasing offset (or p), as predicted by equation 4. However, the resulting shot gather contains significantly fewer P-waves than the original x-component.

The near-surface velocity v_s is even harder to estimate in practice. The equation for S-wave spillover, $u'_{S,l}/u'_{P,l}$, on the l'-component caused by an error in v_s is calculated in an analogous fashion; the result is the same as expression 4 except the P- and S-wave subscripts are reversed. Like P-wave spillover, S-wave spillover exhibits similar relations between percentage error, slowness, and v_p/v_s ratio. However, the separation scheme is less sensitive to v_s error than to v_p error since v_s is always smaller than v_p. Errors up to −45% and +50% in v_s (for $p = 0.4$ s/km, $v_p/v_s = \sqrt{3}$, $v_p = 1.6$ km/s, and $u_{P,tot} = u_{S,tot}$) yield approximately 20% S-wave spillover.

Anisotropic and laterally heterogeneous surface layers

Our scheme assumes a thin isotropic layer at the surface where the velocity is laterally constant. We performed various tests to determine how separation results are affected if this assumption is violated. Lateral P-wave velocity gradients up to 0.25 s^{-1} were introduced in the upper part of the six-layer model. Results show that the separation quality decreases with an increasing gradient, but P-P or P-S wave contamination is always significantly reduced in the resulting shot gathers for P-wave gradients less than approximately 0.125 s^{-1}.

The effect of elliptical P-wave anisotropy in the near-surface layer was also examined. Tests show that the separation quality degrades with increasing anisotropy but remain reasonable for values up to 20% anisotropy. In the case of elliptical anisotropy, the vertical and horizontal P-wave velocities differ, but moveout remains hyperbolic (Thomsen, 1986). The effect on nonelliptical anisotropy is harder to anticipate but probably restricts performance to somewhat smaller amounts of anisotropy.

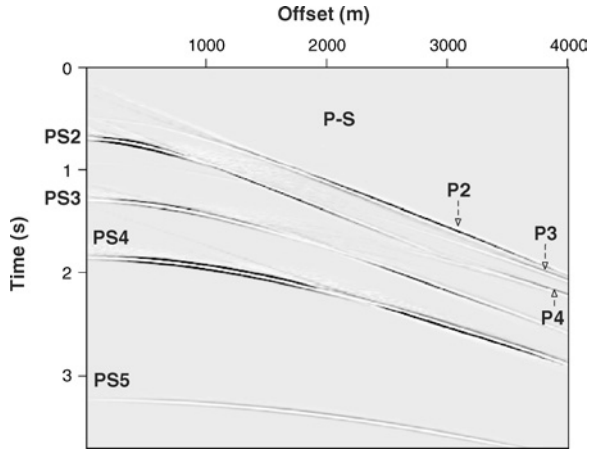

Figure 3. Resulting P-S shot gather after overestimating the near-surface v_p by 20%. More P-wave energy has leaked into the new shot gather, but the S/N ratio is still significantly better than the original x-component (compare with Figures 2b and 2h).

APPLICATION TO REAL DATA

We examine the applicability of the separation scheme to real data from western Canada. The data set was acquired over a sedimentary basin where the geologic structure is roughly flat. Only basic processing was applied on the shot gathers: top mute, bandpass filtering, and scaling of the amplitudes with time squared to approximately correct for geometric spreading. The latter was done to preserve the relative amplitude ratio between the x- and z-components.

The surface layer v_p was obtained from moveout analysis of both the direct wave and the first P-reflection, and was found to be 1.7 km/s. The near-surface v_s was more difficult to determine because the low S/N ratio on the x-component rendered the first P-S conversion invisible. After a series of performance tests, v_s was set to 0.9 km/s.

Figure 4 displays the original z- and x-component and the enhanced P-wave and P-S CSGs after separation. Both the P-P and P-S CSGs show a significant increase in the S/N ratio, and many events are stronger and more clearly defined. Contamination of surface waves and noncoherent noise is reduced because the τ-p transform acts as a dip filter. This, in combination with the presence of an antialiasing filter (Moon et al., 1986) in the forward and inverse τ-p transform, leads to smoother events. The resulting P-P gather displays a higher increase in S/N ratio than the P-S gather. One drawback of the method is that the S/N ratio in one component may be affected by the S/N ratio in the other one. For instance, energy from the z-component (e.g., at $x = 2$ km and $t = 1.1$ s) leaked into the P-S gather after separation.

The leakage of P-waves into the P-S gather could also be caused by the presence of nonlinearly polarized P- and S-waves. Indeed, hodogram analysis shows that both wave types display some elliptical particle motion. This could be the result of multipathing and overlapping arrivals such as local conversions at the surface. In practice, this effect is most prominent at large offset/depth ratios that are normally muted out.

DISCUSSION AND PRACTICAL REQUIREMENTS

The near-surface needs to be approximately laterally homogeneous for our technique to work well. In addition, care should be taken to ensure that neither processing nor acquisition affects the relative ratio between the horizontal and vertical ground displacement. The latter condition requires care in applying gain methods to ensure that this ratio is not changed. For instance, automatic gain control should not be used prior to wavefield separation. Furthermore, relative horizontal and vertical geophone coupling, sensitivity, and calibration all affect the performance. An elevation correction also needs to be applied.

Single geophone recording (one geophone per recording channel) is desirable. The separation quality may degrade if geophone groups are used without further correction, since this again affects the polarization directions. See Dankbaar (1985) for a thorough discussion.

Our scheme is based on a rotation by the incidence angle at the receiver and, therefore, uses the receiver slowness. Hence,

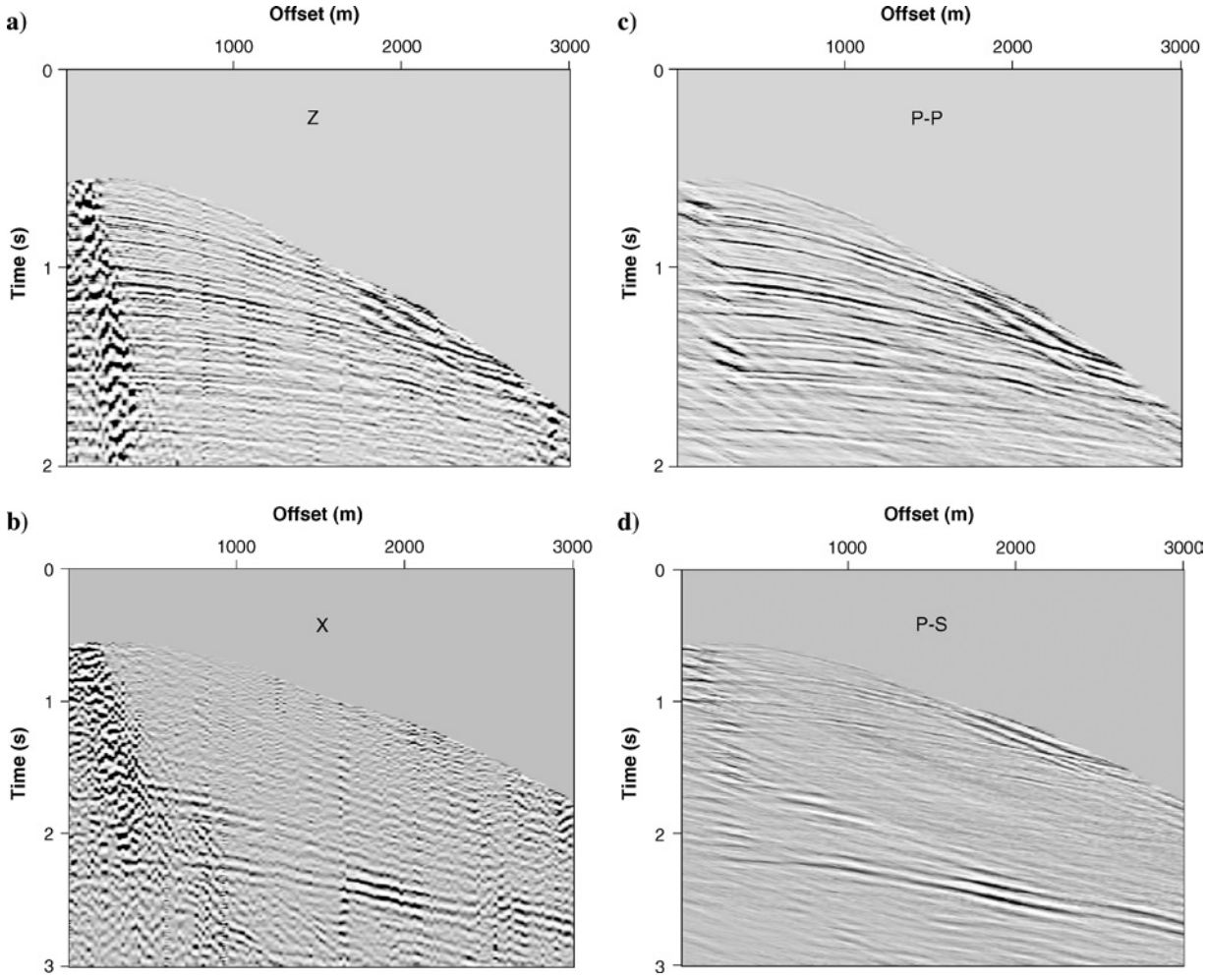

Figure 4. Application on real data. Original shot gathers z-component (a) and x-component (b) and resulting shot gathers P-P (c) and P-S (d) after separation using, respectively, the near-surface v_s and v_p velocities. In particular, the P-P section shows a significantly improved S/N ratio. Note that time scales are different on top and bottom.

it needs to be applied on CSGs instead of common-midpoint or common-receiver gathers.

The use of a constant velocity in the separation scheme can be a limitation for seismic lines that run over areas where the near surface exhibits large lateral variations in elastic properties. However, mild lateral variation in the surface layer within a spread length can be accounted for by rescaling the data during the τ-p transform [see Greenhalgh et al. (1990) for details].

CONCLUSIONS

Our approximate τ-p domain wavefield-separation scheme yields significantly higher S/N ratios in both P-P and P-S shot gathers of both synthetic and real data. This is achieved by a simple rotation based on a single near-surface velocity, thereby effectively removing most energy from contaminating modes. Our approximate separation scheme gives us the freedom of choice to remove either the P-waves or, conversely, superposed converted waves from a multicomponent data set by specifying a single velocity. This is in strong contrast to exact wavefield-separation schemes that attempt to solve both situations simultaneously. These require the specification of both P- and S-wave velocities and often density, with performance strongly depending on the accuracy of each single parameter. Our scheme is applicable to a laterally inhomogeneous anisotropic earth with a homogeneous isotropic surface layer. Sensitivity tests show that errors in the estimates of the near-surface P- and S-wave velocities can be as much as 20% and 45%, respectively, while still obtaining satisfactory results. Also, reasonable results can be attained with near-surface elliptical anisotropy and lateral velocity gradients of as much as 20% and 0.125 s^{-1}, respectively.

ACKNOWLEDGMENTS

We thank Veritas for permission to use their seismic data and Petroleum Development Oman (PDO) for financial support. We also thank S. Greenhalgh and two anonymous reviewers for their constructive comments.

REFERENCES

Amundsen, L., and A. Reitan, 1995, Decomposition of multicomponent sea-floor data into upgoing and downgoing P- and S-waves: Geophysics, **60**, 563–572.

Cho, W. H., and T. W. Spencer, 1992, Estimation of polarization and slowness in mixed wavefields: Geophysics, **57**, 805–814.

Dankbaar, J. W. M., 1985, Separation of P- and S-waves: Geophysical Prospecting, **33**, 970–986.

Esmersoy, C., 1990, Inversion of P and SV waves from multicomponent offset vertical seismic profiles: Geophysics, **55**, 39–50.

Greenhalgh, S. A., I. M. Mason, E. Lucas, D. Pant, and R. T. Eames, 1990, Controlled direction reception filtering of P- and S-waves in τ-p space: Geophysical Journal International, **100**, 221–234.

Guest, S., and M. Kendall, 1993, Modelling seismic waveforms in anisotropic inhomogeneous media using ray and Maslov asymptotic theory: Applications to exploration seismology: Canadian Journal of Exploration Geophysics, **29**, 78–92.

Moon, W., A. Carswell, R. Tang, and C. Dillistone, 1986, Radon transform wave field separation for vertical seismic profiling data: Geophysics, **51**, 940–947.

Richwalski, S., K. Roy-Chowdhury, and J. C. Mondt, 2000, Practical aspects of wave-field separation of two-component surface seismic data based on polarisation and slowness estimates: Geophysical Prospecting, **48**, 697–722.

Stoffa, P. L., P. Buhl, J. B. Diebold, and F. Wenzel, 1981, Direct mapping of seismic data to the domain of intercept time and ray parameter — A plane-wave decomposition: Geophysics, **46**, 255–267.

Thomsen, R. H., 1986, Weak elastic anisotropy: Geophysics, **51**, 1954–1966.

Wang, Y., and S. C. Singh, 2002, Separation of P- and SV-wavefields from multicomponent seismic data in the tau-p domain: Geophysical Journal International, **151**, 633–661.

Wapenaar, C. P., P. Hermann, D. J. Verschuur, and A. J. Berkhout, 1990, Decomposition of multicomponent seismic data into primary P- and S-wave responses: Geophysical Prospecting, **38**, 633–661.